Symposium on Applied Fractional Calculus

Badajoz (Industrial Engineering School), October 15-17, 2007

APLICATION OF FRACTIONAL ALGORITMS
IN THE CONTROL OF AN HELICOPTER SYSTEM

J. Coelho[1], R. Matos Neto[1], C. Lebres[1], H. Fachada[1], N. M. Fonseca Ferreira[1]
E. J. Solteiro Pires[2], J. A. Tenreiro Machado[3]

[1]Polytechnic Institute of Coimbra, Institute of Engineering of Coimbra,
Dept. of Electrical Engineering, Quinta da Nora, Apartado 10057
3031-601 Coimbra Codex, Portugal,
[2]University of Trás-os Montes e Alto-Douro, Dept. of Engineering Quinta de Prados,
Apartado 202, 5000 Vila Real, Portugal
[3] Polytechnic Institute of Porto, Institute of Engineering of Porto,
Rua Dr Ant. Bernardino de Almeida, 4200 − 072 Porto, Portugal
e-mail: joaobcoelho@hotmail.com, e-mail: rofdolfonneto@gmail.com, e-mail:clebres@isec.pt
[1]e-mail: nunomig@isec.pt, [2]e-mail: epires@utad.pt, [3]email: jtm@isep.ipp.pt

Abstract: This paper compares the application of fractional and integer order controllers for a laboratory helicopter twin rotor MIMO system using the MatLab package.

Keywords: Helicopter, Mathematic Model, Position Control, Fractional Control.

1. INTRODUCTION

In this study we consider the dynamics of the helicopter system with two degrees of freedom (2-DOF) [1, 2]. The simulation and the real-time experiments in closed loop are performed and several comparisons are presented.
Figure 1 shows a laboratory model of the Twin Rotor.

Figure 1 - Two views of the twin rotor MIMO System.

At both ends of a beam, there are two propellers driven by DC motors, the beam is joined to its base though with an articulation. The articulated joint allows the beam to rotate so that its ends move on spherical surfaces. A counter-weight fixed to the beam determines a stable equilibrium position. The rotors are positioned perpendicularly to each other, so that the movements in the vertical and horizontal planes are only affected by the thrust one propeller. The controls of the system consist in the supply voltages of the motors. The measured signals are the two position angles that determine the position of the beam in space and the angular velocities of the rotors. The positions are measured using incremental encoders, and the angular velocities are reconstructed by a simple differentiation and a second-order filtering of the measured position angles.

This paper presents several control techniques for a lab helicopter model. It is adopted the Twin Rotor Mimo System (*Feedback* – TRMS) and are compared integer and fractional order control algorithms.
The paper is organize as follow. Section two, provides an overview of the system model. Section three shows the conventional integer and the fractional order algorithms. Section four presents the simulations results. Finally, section five outlines some conclusions.

2. MATHEMATICAL MODEL

First, we consider the rotation of the beam in a vertical plane that is around the horizontal axis.
The helicopter has 2-DOF, the rotation of the helicopter body with respect to the horizontal axis and the rotation around the vertical axis, which are measured by two sensors. Each axis has one potentiometer for measuring the angle. The helicopter can move the horizontal axis, in the range $-170° < \alpha_h < 170°$, and the vertical axis, within $-60° < \alpha_h < 60°$, in pitch. The inputs are the voltages U_h and U_v affecting the main and tail rotor. The output command must match the capabilities of the hardware board that is capable to outputing [0, 5] Volt signal. This signal is shifted in the amplifier to create ±2.5 Volt capability required to command the drive motor in both directions. When no control signals are applied, the helicopter will tend to position at $\alpha_h = -60°$.

Table I – List of symbols

Variable	Description	Units [SI]
α_h	Horizontal position (azimuth position) of the model beam	[rad]
Ω_h	Angular velocity (azimuth velocity) of the model beam	[rad/s]
U_h	Horizontal DC-motor voltage control input	[V]
G_h	Linear transfer function of tail rotor DC-motor	
H	Non-linear part of DC- motor with tail rotor	[rad/s]
ω_h	Rotational speed of tail rotor	[rad/s]
F_h	Non-linear function (quadratic) of aerodynamic force from tail rotor	[N]
l_h	Effective arm of aerodynamic force from tail rotor	[m]
J_h	Non-linear function of moment of inertia with respect to vertical axis	[Kg.m^2]
M_h	Horizontal turning torque	[N.m]
K_h	Horizontal angular momentum	[N.m.s]
f_h	Moment of friction force in vertical axis	[N.m]
α_v	Vertical position (Pitch position) of the model beam	[rad]
Ω_v	Angular velocity (Pitch velocity) of the model beam.	[rad/s]
U_v	Vertical DC-motor voltage control input	[V]
G_v	Linear transfer function of main rotor DC-motor	
v	Non-linear part of DC-motor with main rotor	[rad/s]
ω_v	Rotational speed of main rotor	[rad/s]
F_v	Non-linear function (quadratic) of aerodynamic force from main rotor	[N]
l_v	Arm of aerodynamic force from main rotor	[m]
J_v	Moment of inertia with respect to horizontal axis	[Kg.m^2]
M_v	Vertical turning moment	[N.m]
K_v	Vertical angular momentum	[N.m.s]
f_v	Moment of friction force in horizontal axis	[N.m]
f	Vertical turning moment from counterbalance	[N.m]
J_{hv}	Vertical angular momentum from tail rotor	[N.m.s]
J_{vh}	Horizontal angular momentum from tail rotor	[N.m.s]
g_{vh}	Non-linear function (quadratic) of reaction turning	[N.m]
g_{hv}	Non-linear function (quadratic) of reaction turning	[N.m]
t	Time	[s]
L	Laplace Operator	
z	Transform variable	

The physical model is developed under some simplifying assumptions. It is assumed that friction is of the viscous type and that the propeller air subsystem can be described in accordance with the postulates of flow theory.

First, we consider the rotation of the beam in the vertical plane, around the horizontal axis. Having in mind that the driving torques are produced by the propellers, the rotation can be described in principle as the motion of a pendulum. From the Newton second law of motion we obtain:

$$M_v = J_v \frac{d^2\alpha_v}{dt^2} \qquad (1)$$

$$M_v = \sum_{i=1}^{4} M_{vi} \qquad (2)$$

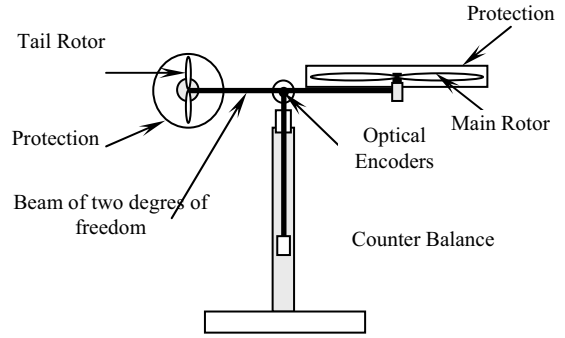$$J_v = \sum_{i=1}^{8} J_{vi} \qquad (3)$$

Figure 2 – The twin rotor mimo system.

To determine the moments of gravity applied to the beam, making it rotate around the horizontal axis, we consider the situation of in figure 3, and:

$$M_{v1} = g[A - B]\cos\alpha_v - C\sin\alpha_v \qquad (4a)$$

$$A = \left(\frac{m_t}{2} + m_{tr} + m_{ts}\right)l_t \qquad (4b)$$

$$B = \left(\frac{m_m}{2} + m_{mr} + m_{ms}\right)l_m \qquad (4c)$$

$$C = \frac{m_b}{2}l_b + m_{cb}l_{cb} \qquad (4d)$$

Table II – The parameters of the Helicopter.

Variable	Value	Units [SI]
m_{mr}	0.228	[kg]
m_m	0.0145	[kg]
m_{tr}	0.206	[kg]
m_t	0.10166	[kg]
m_{cb}	0.068	[kg]
m_b	0.022	[kg]
m_{ms}	0.225	[kg]
m_{ts}	0165	[kg]
l_m	0.24	[m]
l_t	0.25	[m]
l_b	0.26	[m]
l_{cb}	0.13	[m]
r_{ms}	0.155	[m]
r_{ts}	0.10	[m]

where r_{ms} is the radius of the main shield and r_{ts} is the radius of the tail shield.

Also:

$$M_{v2} = l_m F_v(\omega_m) \qquad (5)$$

where $F_v(\omega_m)$ denotes the dependence of the propulsive force on the angular velocity of the rotor.

$$M_{v3} = -\Omega_h^2 (A + B + C) \sin\alpha_v \cos\alpha_v \qquad (6)$$

$$\Omega_h = \frac{d\alpha_h}{dt} \qquad (7)$$

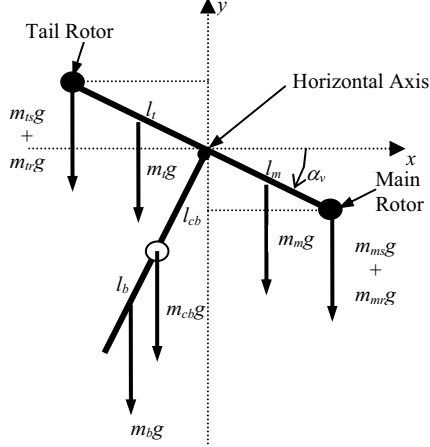To determine the moments of propulsive forces applied to the beam consider the situation given in figure 3.

Figure 3 – Gravity forces in the TRMS, corresponding to the return torque, which determines the equilibrium position of the system.
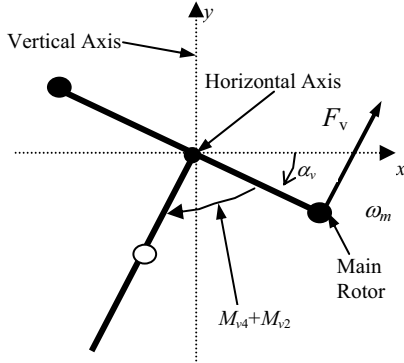
Finaly:

$$M_{v4} = -\Omega_v K_v \qquad (8)$$

Figure 4 – Propulsive force moment and friction moment in the TRMS.

$$\Omega_v = \frac{d\alpha_{vh}}{dt} \qquad (9)$$

where Ω_v is the angular velocity around the horizontal axis and K_v is a constant.

According to figure 4 we can determine components of the moment of inertia relative to the horizontal axis. Notice, that this moment is independent of the position of the beam.

$$J_{v1} = m_{mr} l_m^2 \qquad (10a)$$

$$J_{v2} = m_m \frac{l_m^2}{3} \qquad (10b)$$

$$J_{v3} = m_{cb} l_{cb}^2 \qquad (10c)$$

$$J_{v4} = m_b \frac{l_b^2}{3} \qquad (10d)$$

$$J_{v5} = m_{tr} l_t^2 \qquad (10e)$$

$$J_{v6} = m_t \frac{l_t^2}{3} \qquad (10f)$$

$$J_{v7} = \frac{m_{ms}}{2} r_{ms}^2 + m_{ms} l_m^2 \qquad (10g)$$

$$J_{v8} = m_{ts} r_{ts}^2 + m_{ts} l_t^2 \qquad (10h)$$

Similarly, we can describe the motion of the beam around the vertical axis, having in mind that the driving torques are produced by the rotors and that the moment of inertia depends on the pitch angle of the beam. The horizontal motion of the beam (around the vertical axis) can be described as a rotational motion of a solid mass:

$$M_h = J_h \frac{d^2\alpha_h}{dt^2} \qquad (11a)$$

$$M_h = \sum_{i=1}^{2} M_{hi} \qquad (11b)$$

$$J_h = \sum_{i=1}^{8} J_{hi} \qquad (11c)$$

To determine the moments of forces applied to the beam and making it rotate around the vertical axis, consider the situation shown in Figure 5.

$$M_{h1} = l_t . F_h(w_t) \cos\alpha_v \qquad (12)$$

where $F_h(\omega_t)$ denotes the dependence of propulsive force on the angular velocity of the tail rotor which should be determined experimentally, and:
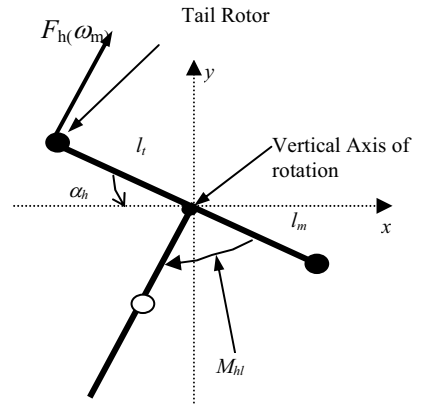

Figure 5 - Moments of forces in horizontal plane.

$$M_{h2} = -\Omega_h K_h \qquad (13)$$

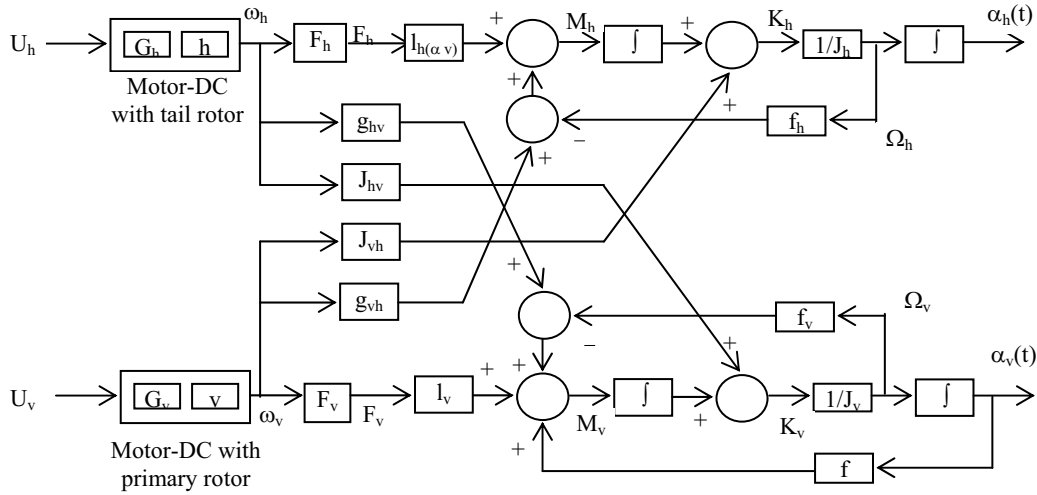$$J_h = D \cos^2\alpha_v + E \sin^2\alpha_v + F \qquad (14)$$

Figure 6 – The MIMO Block Diagram of the Twin Rotor

$$D = \frac{m_b}{3} l_b^2 + m_{cb} l_{cb}^2 \qquad (15)$$

$$E = \left(\frac{m_m}{3} + m_{mr} + m_{ms}\right) l_m^2 + \left(\frac{m_t}{3} + m_{tr} + m_{ts}\right) l_t^2 \qquad (16)$$

$$F = m_{ms} r_{ms}^2 + \frac{m_{ts}}{2} r_{ts}^2 \qquad (17)$$

The helicopter motion can be describe by the equations:

$$\frac{dS_v}{dt} = \frac{l_m F_v(\omega_m) - \Omega_v K_v + G - H}{J_v} \qquad (18a)$$

$$G = g\left[(A - B)\cos\alpha - C\sin\alpha_v\right] \qquad (18b)$$

$$H = \frac{1}{2}\Omega_h^2(A + B + C)\sin 2\alpha_v \qquad (18c)$$

$$\frac{d\alpha_v}{dt} = \Omega_v \qquad (18d)$$

$$\Omega_v = \frac{S_v + J_{tr}\omega_t}{J_v} \qquad (18e)$$

$$\frac{dS_h}{dt} = \frac{l_t F_h(\omega_t)\cos\alpha_v - \Omega_h K_h}{J_h} \qquad (18f)$$

$$\Omega_h = \frac{d\alpha_h}{dt} \qquad (18g)$$

$$\Omega_h = S_h + \frac{J_{tmr}\omega_m\cos\alpha_v}{J_h} \qquad (18h)$$

The angular velocities are a function of the DC motors, yielding:

$$\frac{du_{vv}}{dt} = \frac{1}{T_{mr}}(-u_{vv} + u_v) \qquad (19a)$$

$$\omega_m = P_v(u_{vv}) \qquad (19b)$$

$$\frac{du_{hh}}{dt} = \frac{1}{T_{tr}}(-u_{hh} + u_h) \qquad (19c)$$

$$\omega_t = P_h(u_{hh}) \qquad (19d)$$

Finally, the mathematical model becomes a set of six non-linear equations, namely:

$$\mathbf{U} = [U_h \ U_v]^T \qquad (20)$$

$$\mathbf{X} = [S_h \ \alpha_h \ u_{hh} \ S_v \ \alpha_v \ u_{vv}]^T \qquad (21)$$

$$\mathbf{Y} = [\Omega_h \ \alpha_h \ \omega_t \ \Omega_v \ \alpha_v \ \omega_m]^T \qquad (22)$$

where **U** is the input, **X** is the state and **Y** is the output vector.

3. TWIN ROTOR MIMO CONTROLLERS

3.1. INTEGER ORDER ALGORITHMS

The *PID* controllers are the most commonly used control algorithms in industry. Among the various existent schemes for tuning *PID* controllers, the Ziegler-Nichols (Z-N) method is the most popular and is still extensively used for the determination of the PID parameters. It is well known that the compensated systems, with controllers tuned by this method, have generally a step response with a high percent overshoot. Moreover, the Z-N heuristics are only suitable for plants with monotonic step response [5-7].
The transfer function of the PID controller is:

$$G_c(s) = \frac{U(s)}{E(s)} = K\left(1 + \frac{1}{T_i s} + T_d s\right) \qquad (23)$$

where $E(s)$ is the error signal and $U(s)$ is the controller's output. The parameters K, T_i, and T_d are the proportional gain, the integral time constant and the derivative time constant of the controller, respectively.

The design of the *PID* controller consist on the determination of the optimum *PID* gains (K, T_i, T_d) that minimize J, the integral of the square error (ISE), defined as:

$$J = \int_0^\infty \left\{ [\alpha_h(t) - \alpha_{hd}(t)]^2 + [\alpha_v(t) - \alpha_{vd}(t)]^2 \right\} dt \qquad (24)$$

where $\alpha_i(t)$ is the step response of the closed-loop system with the *PID* controller and $\alpha_{id}(t)$ is the desired step response.

The control architecture can be resumed in the block diagram of Figure 7, with the two independent controllers.
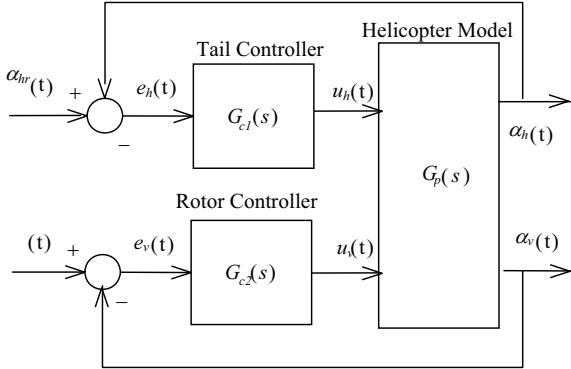

Figure 7 –Twin Rotor Mimo Block *PID* Control Diagram.

3.2. FRACTIONAL ORDER ALGORITHMS

In this section we present the *FO* algorithms inserted at the position loops.

The mathematical definition of a derivative of fractional order α has been the subject of several different approaches. For example, we can mention the Laplace and the Grünwald-Letnikov definitions:

$$D^\alpha[x(t)] = L^{-1}\{s^\alpha X(s)\} \qquad (25a)$$

$$D^\alpha[x(t)] = \lim_{h \to 0} \left[\frac{1}{h^\alpha} \sum_{k=1}^{\infty} \frac{(-1)^k \Gamma(\alpha+1)}{\Gamma(k+1)\Gamma(\alpha-k+1)} x(t-kh) \right] \qquad (25b)$$

where Γ is the gamma function and h is the time increment.

In our case, for implementing *FO* algorithms of the type $C(s) = K_P + \dfrac{K_I}{T_i s} + K_D\, s^\alpha, -1 < \alpha < 1$, we adopt a 4th-order discrete-time Pade approximation ($a_i, b_i, c_i, d_i \in \Re, k = 4$):

$$C_{Ph}(z) \approx K_{Ph} \frac{a_0 z^k + a_1 z^{k-1} + .. + a_k}{b_0 z^k + b_1 z^{k-1} + ... + b_k} \qquad (26a)$$

$$C_{Pv}(z) \approx K_{Pv} \frac{c_0 z^k + c_1 z^{k-1} + .. + c_k}{d_0 z^k + d_1 z^{k-1} + ... + d_k} \qquad (26a)$$

where K_{Ph} and K_{Pv} are the position main and tail gains, respectively.

4. CONTROLLER PERFORMANCES

This section analyzes the system performance; furthermore, we compare the response of classical *PID* and *PID*$^\alpha$ controllers.

For the *PID* integer – order case we adopt:

Table I –The *PID* gains.

Parameters	Main	Tail
K_P	14.5	10.0
K_I	10.7	3.7
K_D	7.0	8.0

For the *PID*$^\alpha$ factional–order case we adopt:

Table II – The *PID*$^\alpha$ control gains.

Parameters	Main	Tail
K_P	14.5	10.0
K_I	10.7	3.7
K_D	7.0	8.0
α	0.7	0.7

In order to study the system dynamics we apply separately, rectangular pulses, at the tail and main rotor, that is, we perturb the reference with $\{\delta\alpha_h, \delta\alpha_v\} = \{12°, 0\}$ and $\{\delta\alpha_h, \delta\alpha_v\} = \{0°, 12°\}$. These perturbations have a duration of 15 seconds.

In the first experimental test, to choose the sample time of the system we consider three different values of samples. Figure 8 and tables III and IV show the analysis of the time response characteristics, for the tail and the rotor perturbations. Figure 9 illustrate the quadratic error response for the trajectory perturbation. Figures 11 and 12 demonstrate for different sampling times the required voltages U_v and U_h to execute the same task. After this analysis we observe that the $h = 0.01$ s is the more adequated value, because it requires a smaller control actions and leads to smaller errors.

The second group of experiment shows the effect of changing of the α parameters of both the main and the tail rotors. Figures 13 and 14 present this results and reveal that the range of the α parameters [0.6, 1] produce smaller errors, and need less energy to perform the task. Therefore, for the *PID*$^\alpha$ we adopt $\alpha_h = \alpha_v = 0.7$.

In order to compare the *PID* and *PID*$^\alpha$, we repeat the experiments, by introducing an perturbation corresponding to two different loads, and we analyze the results. The *PID*$^\alpha$ controller reveals better performance, namely is faster and produces small errors than the *PID*.
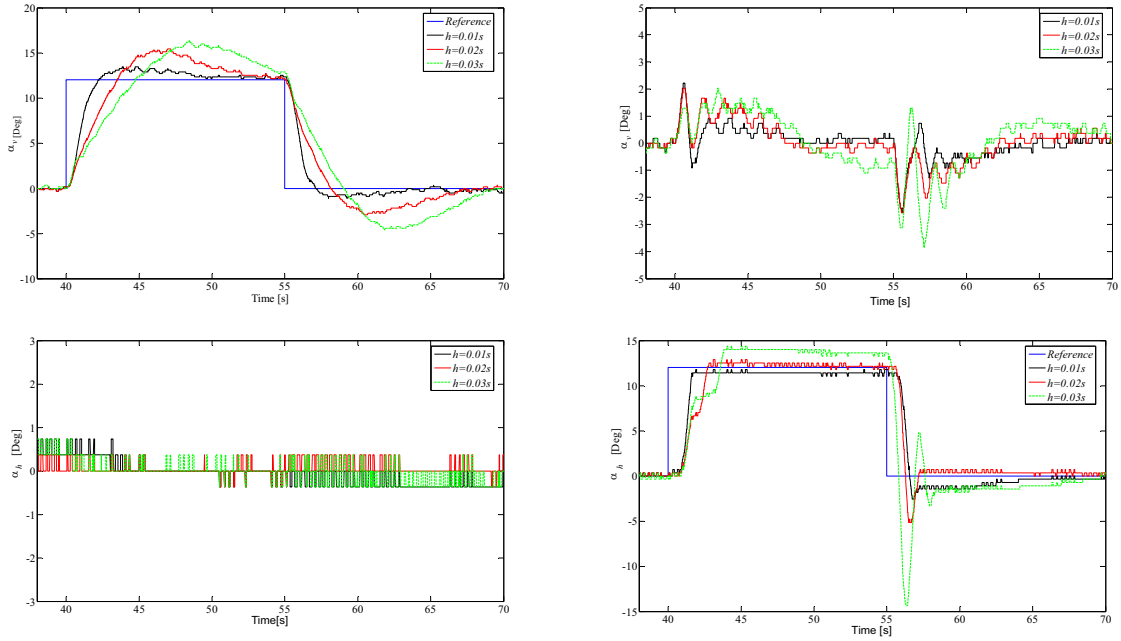
Figure 8 – Time response of α_v and α_h using the PID^α controllers, for a pulse perturbation at the α_{hr} and α_{vr} position reference $\delta\alpha_h = 12^\circ$ for different sampling times $h = \{0.01, 0.02, 0.03\}$.
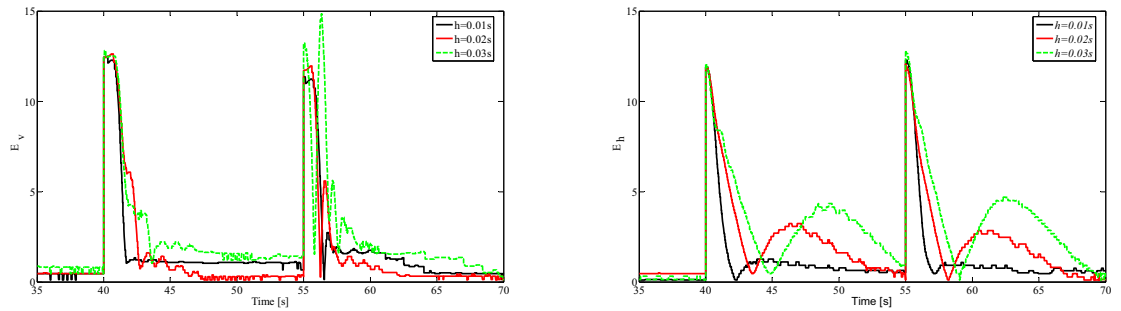

Figure 9 – Time response of quadratic error $\varepsilon_{h,v}$ for trajectory perturbation, at α_v and α_h using the PID^α controllers, for a pulse perturbation at the α_{hr} and α_{vr} position references $\delta\alpha_h = 12^\circ$ and $\delta\alpha_v = 12^\circ$ for different sampling times $h = \{0.01, 0.02, 0.03\}$.
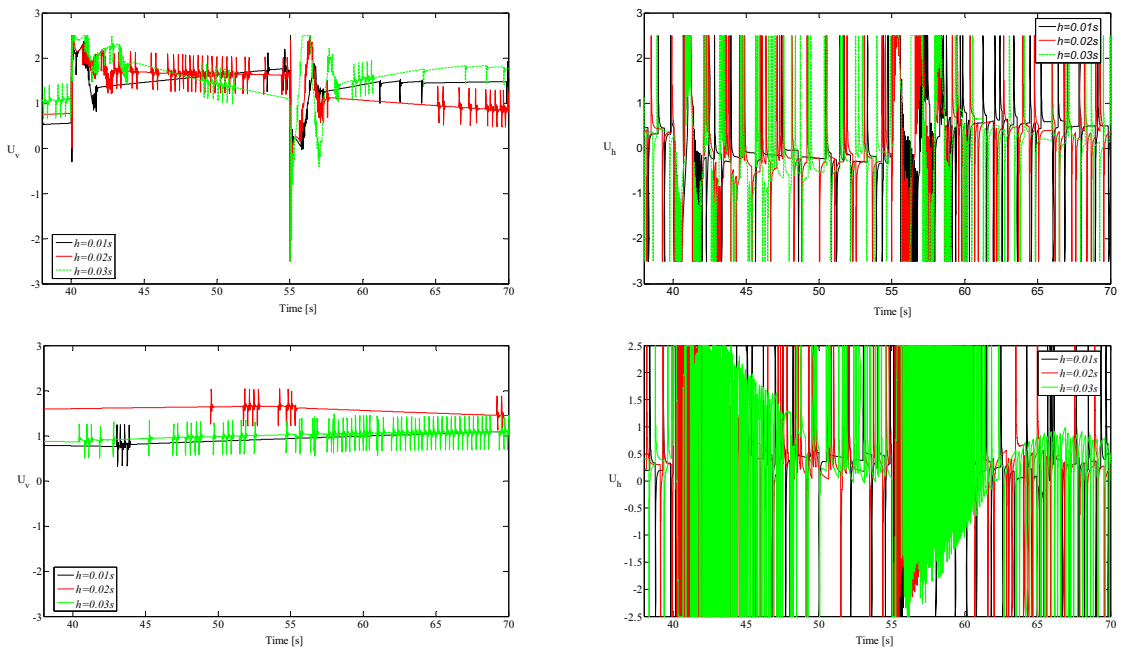
Figure 10 – Time response of U_h and U_v using the PID^α controllers, for a pulse perturbation at the α_{hr} position reference $\delta\alpha_h = 12^\circ$ and $\delta\alpha_v = 12^\circ$ for different sampling times $h = \{0.01, 0.02, 0.03\}$.
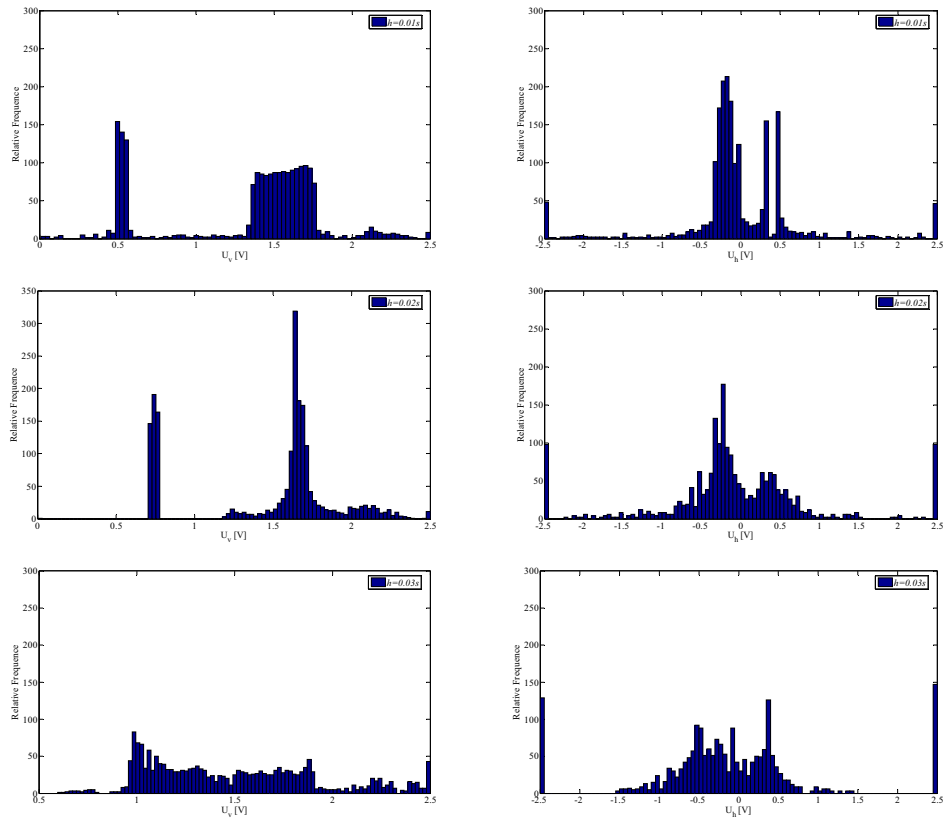
Figure 11 − Rotor and tail voltage statistical distribution using the PID^{α} controllers, for a pulse perturbation $\delta\alpha_v = 12^{\circ}$ at the α_{vr} position reference for different sampling times $h = \{0.01, 0.02, 0.03\}$.
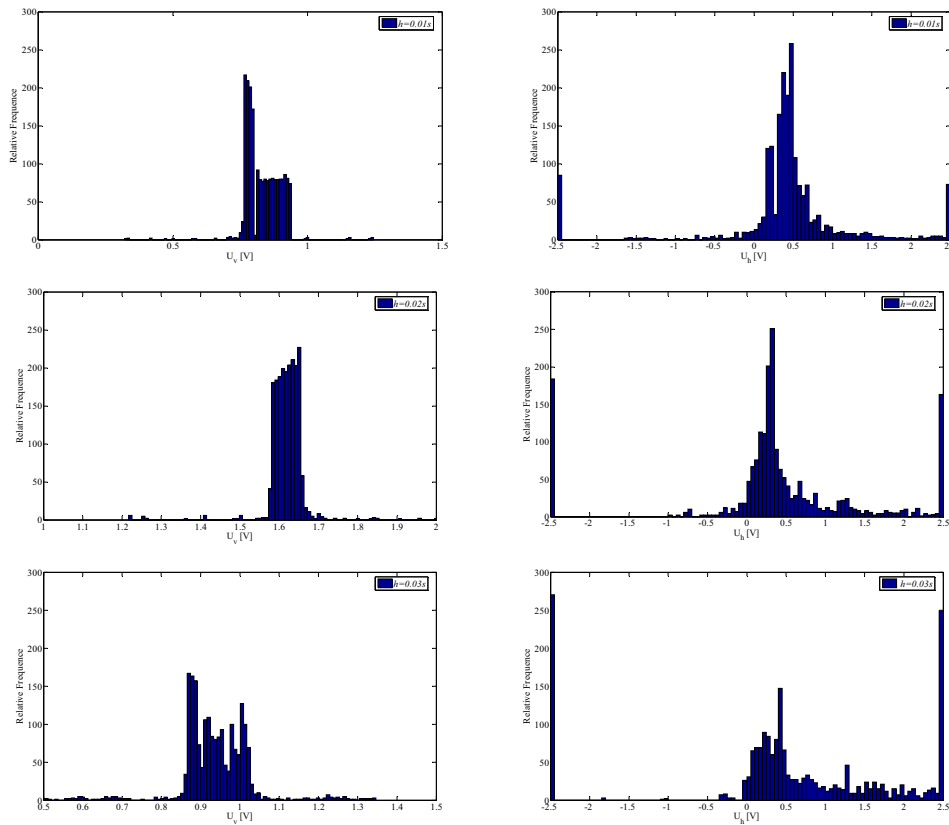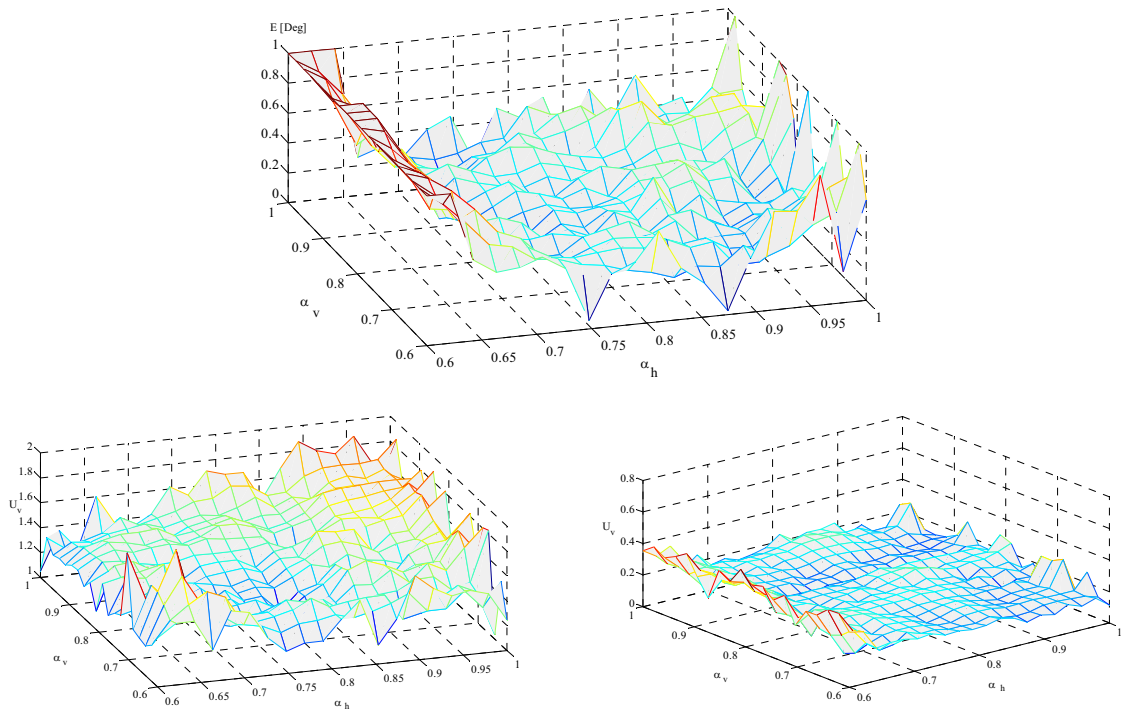

Figure 12 − Rotor and tail voltage statistical distribution using the PID^{α} controllers, for a pulse perturbation $\delta\alpha_h = 12^{\circ}$ at the α_{hr} position reference for different sampling times $h = \{0.01, 0.02, 0.03\}$.
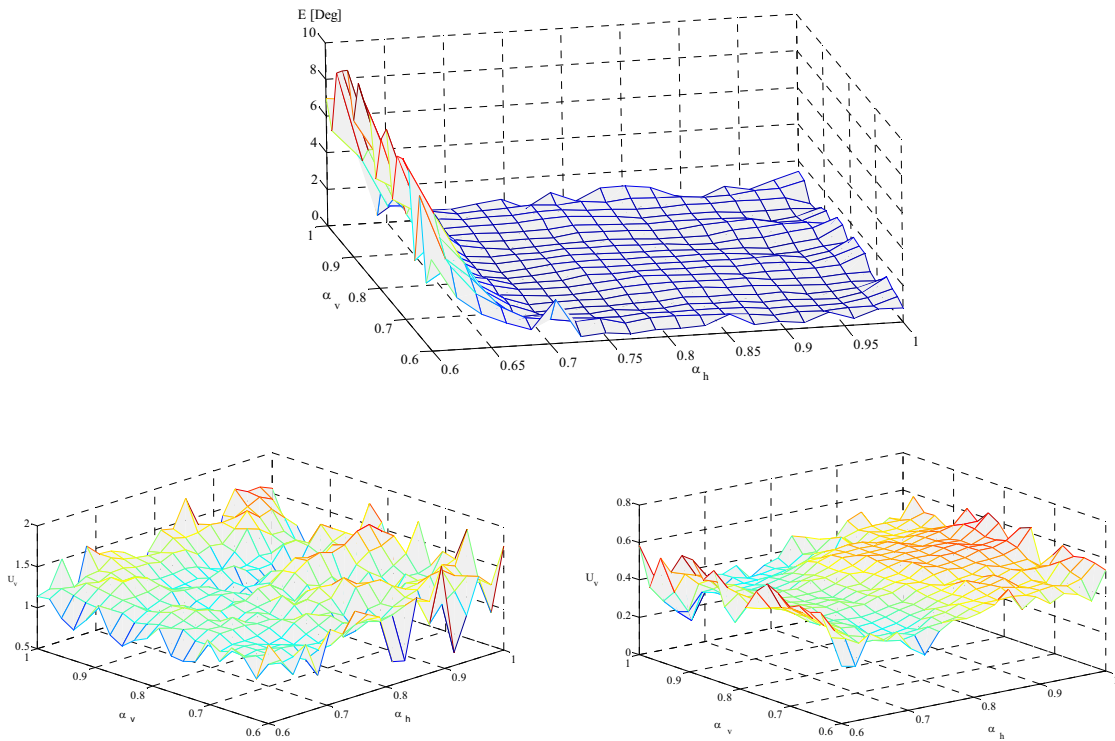
Figure 13 – The quadratic error $\varepsilon_{h,v}$, the main and tail rotor mean voltages U_v and U_h using the PID^α controllers, for a pulse perturbation at the α_{hr} position reference $\delta\alpha_h = 12º$ for different values of α_h and α_v in the PID^α controllers.

Figure 14 – The quadratic error $\varepsilon_{h,v}$, the rotor and tail rotor mean voltages U_v and U_h using the PID^α controllers, for a pulse perturbation at the α_{vr} position reference $\delta\alpha_v = 12º$ for different value of α_h and α_v in the PID^α controllers.
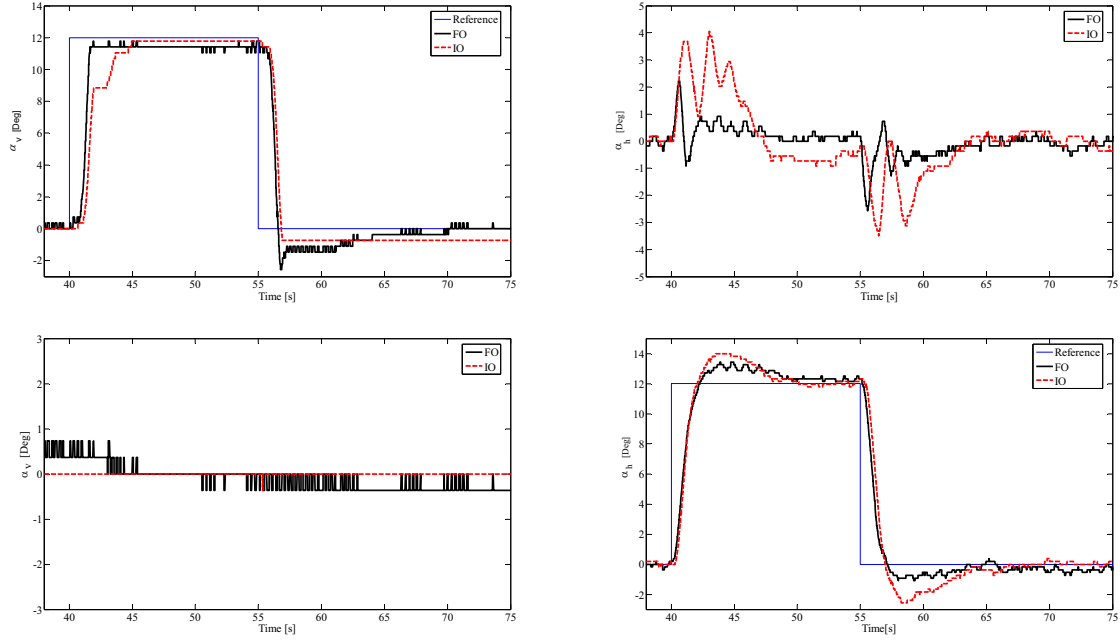
Figure 15 – Time responses of α_v and α_h using the *PID* and *PID*$^\alpha$ controllers, for a pulse perturbation at the α_{hr} position reference $\delta\alpha_h = 12^\circ$ and $\delta\alpha_v = 12^\circ$.

Table III. Time response characteristics for a rectangular pulse $\delta\alpha_v$ at the reference.

	i	PO%	ess	Tp	Ts
PID$^\alpha$	1	1.820	1.00	1.61	1.70
PID$^\alpha$	2	3.20	1.00	2.40	2.50
PID$^\alpha$	3	16.50	1.00	3.50	3.60

Table IV. Time response characteristics for a rectangular pulse $\delta\alpha_h$ at the reference.

	i	PO%	ess	Tp	Ts
PID$^\alpha$	1	11.98	1.00	1.79	9.50
PID$^\alpha$	2	25.05	1.00	3.50	14.5
PID$^\alpha$	3	33.10	1.00	5.00	25.5

Table V. Time response characteristics for a rectangular pulse $\delta\alpha_v$ at the reference.

	PO%	ess	Tp	Ts
PID	41.12	1.00	1.77	3.40
PID$^\alpha$	1.820	1.00	1.61	1.70

Table VI. Time response characteristics for a rectangular pulse $\delta\alpha_h$ at the reference.

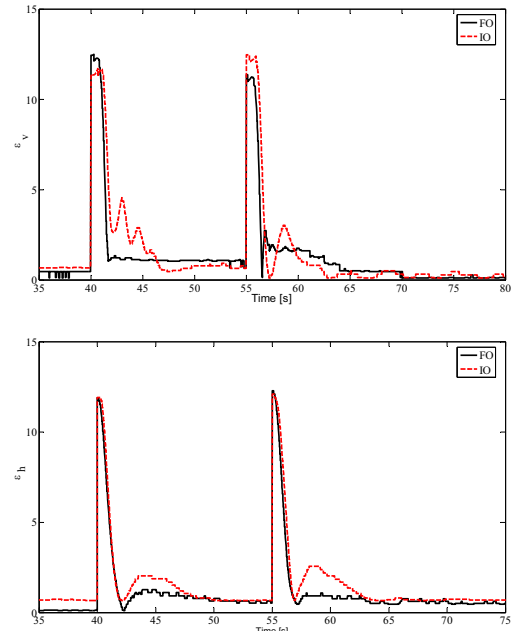|	PO%	ess	Tp	Ts
PID	39.59	1.00	1.25	6.10
PID$^\alpha$	11.98	2.00	1.79	9.50

Figure 16 – Time response of quadratic error $\varepsilon_{h,v}$ for a trajectory perturbation, at α_v and α_h using the *PID* and *PID*$^\alpha$ controllers, for a pulse perturbation at the α_{hr} and α_{vr} position references $\delta\alpha_h = 12^\circ$ and $\delta\alpha_v = 12^\circ$.
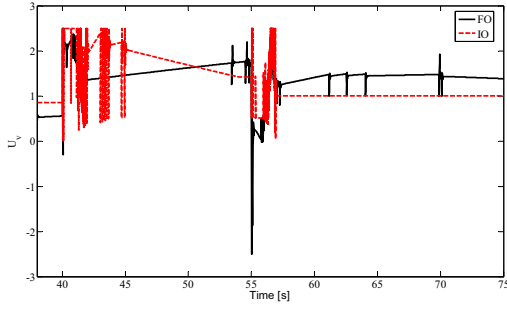
Figure 17 – Time response of U_h using the *PID* and the *PID*$^\alpha$ controllers, for a pulse perturbation at the α_{hr} position reference $\delta\alpha_h = 12°$.
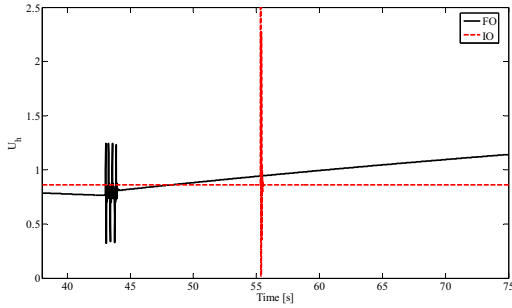

Figure 18 – Time response of U_v using the *PID* and the *PID*$^\alpha$ controllers, for a pulse perturbation at the α_{vr} position reference $\delta\alpha_v = 12°$.
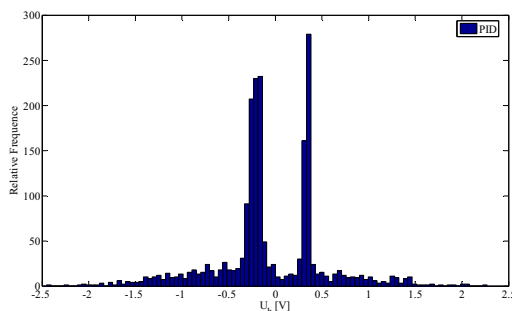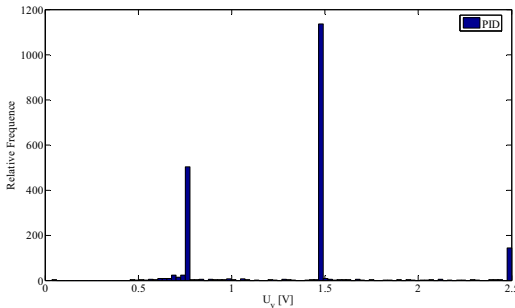

Figure 19 – Rotor and tail voltage statistical distributions using the *PID*, for a pulse perturbation at the position reference $\delta\alpha_v = 12°$ for sampling time $h = 0.01s$.
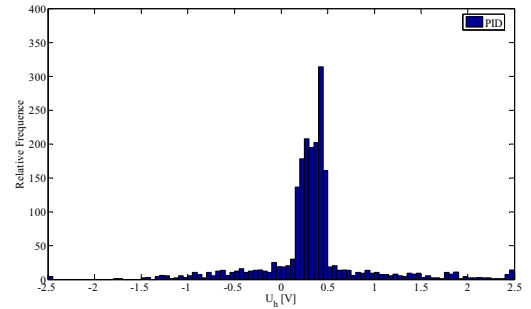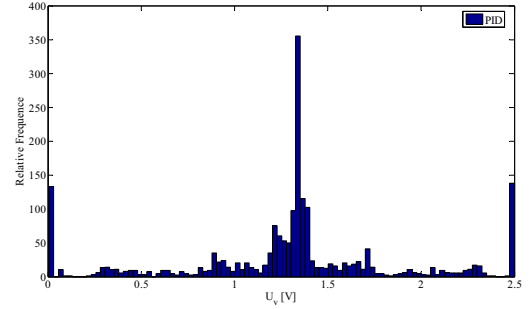

Figure 20 – Rotor and tail voltage statistical distributions using the *PID*, for a pulse perturbation at the position reference $\delta\alpha_h = 12°$ for sampling time $h = 0.01s$.

Table VII. Statistical analysis for a rectangular pulse $\delta\alpha_v$ at the reference.

	$V_v(Mean)$	$V_h(Mean)$	σ_v	σ_h
PID	1.3353	-0.06	0.4802	0.5800
PID$^\alpha$	1.3200	-0.03	0.5000	0.7491

Table VIII. Statistical analysis for a rectangular pulse $\delta\alpha_h$ at the reference.

	$V_v(Mean)$	$V_h(Mean)$	σ_v	σ_h
PID	1.300	0.338	0.5900	0.5470
PID$^\alpha$	0.834	0.420	0.0660	0.8386

In the next group of experiments we introduce two different loads at the ends of the beam, under the DC motor, near the main rotor. The two external loads have mass $M_1 = 0.0149$ Kg and $M_2 = 0.0298$ Kg. The maxim use weight capability of the main rotor is 0.150 Kg (tested in the lab with a dynamometer). Figure 21 and 22 show the time responses of α_v and U_v for these perturbations.
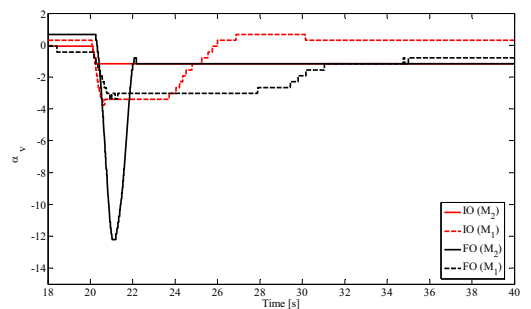

Figure 21 – Time response of α_v using the *PID* and the *PID*$^\alpha$ for a external perturbation at the α_{hr} position reference for $M_1 = 0.0149$ Kg and $M_2 = 0.0298$ Kg.
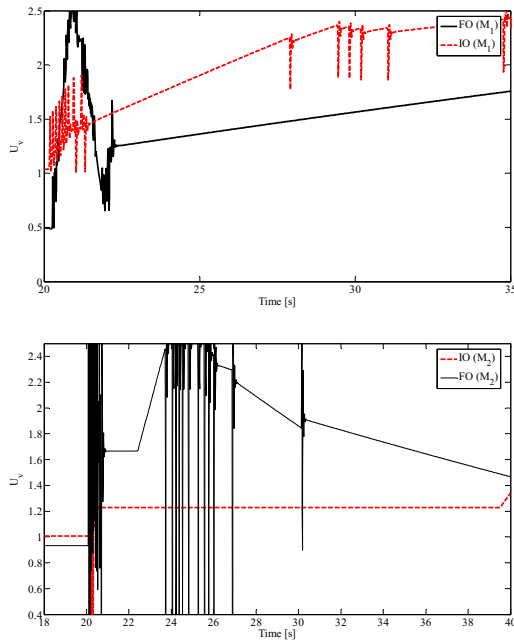
Figure 22 – Time response of U_v using the *PID* and the *PID*$^\alpha$ for a external perturbation at the α_{hr} position reference for M_1 = 0.0149 Kg and M_2 = 0.0298 Kg

We observe that before the external perturbation the consumption of the *PID*$^\alpha$ controller is a reduced amount of energy than the *PID* to perform the same task. Nevertheless, after the introduction of one perturbation at h = 20 seconds, the main controller needs to compensate the perturbation and in the case of *PID*$^\alpha$ controller requires more energy than the *PID*.

5. CONCLUSIONS

In this paper a two rotor MIMO helicopter system is studied and experimented. The mathematical model of TRMS is derived, and its dynamical characteristics, such as equilibrium position, propeller thrust and gravity compensation are analyzed. For this system are compared integer and fractional order algorithms. The results of the *PID*$^\alpha$ controller reveal better performances than the classical controller. The performances are evaluated by introducing a small perturbation at the reference and an external load perturbation. The results demonstrate a good performance for the *PID*$^\alpha$ controller.

REFERENCES

[1] J. Gordon Leishman, *Principles of Helicopter Aerodynamics*, Second Edition, Cambridge University Press.

[2] Martin D. Maisel, Demo J. Giulianetti and Daniel C. Dugan, *The History of the XV-15 Tilt Rotor Research Aircraft From Concept to Flight*, National Aeronautics and Space Administration Office of Policy and Plans NASA History Division Washington, D.C.2000.

[3] Feedback Instruments *Ltd. Manual: 33-007-1C* Ed04, 2002.

[4] M. López Martínez, F.R. Rubio (2004), *Approximate Feedback Linearization of a Laboratory Helicopter*, Sixth Portuguese Conference on Automatic Control, pp.43-45, Faro, Portugal

[5] Islam, B.U.; Ahmed, N.; Bhatti, D.L.; Khan, S., *Controller design using fuzzy logic for a twin rotor MIMO system*, Multi Topic Conference, 2003. INMIC2003. 7th Internationa,lVolume , Issue , 8-9 Dec. 2003 Page(s): 264 – 268.

[6] Przemysław Gorczyca, Krystyn Hajduk, *Tracking Control Algorithms For A Laboratory Aerodynamical System*, Int. J. Appl. Math. Comput. Sci., 2004, Vol. 14, No. 4, 469–475.

[7] Rahideh, A, Shaheed, M H, Proceedings of the I MECH E Part I Journal of Systems & Control Engineering, Volume 221, Number 1, January 2007 , pp. 89-101(13)

[8] Amaral, T.G.; Crisostomo, M.M.; Pires, V.F., *Helicopter motion control using adaptive neuro-fuzzy inference controller*, IEEE IECON 02 Volume: 3 , 5-8 Nov. 2002 , Page(s): 2090 -2095 vol.3

[9] Åström, K., Hang, C., Persson, P. and Ho,W. (1992). *Towards intelligent PID control*, Automática 28(1): 1–9.

[10] Åström, K. J. and Hägglund, T. (1995). *PID controller-Theory, Design and Tuning*, second edn, Instrument Society of America, 67 Alexander Drive, POBox 12277, Research Triangle Park, North Carolina 27709, USA.

[11] Åström, K. J. and Wittenmark, B. (1984). *Computer Controlled Systems, theory and Design*, Prentice-Hall, Englewood Cliffs.

[12] Siler, W. and Ying, H. (1989). *Fuzzy control theory: The linear case*, Fuzzy Sets and Systems 33: 275–290.

[13] Tso, S. K. and Fung, Y. H. (1997). *Methodological development of fuzzy-logic controllers from multivariable linear control*, IEEE Trans. Systems Man & Cybernetics 27(3): 566–572.

[13] Podlubny, *Fractional Differential Equations,* Academic Press, San Diego, 1999.

[14] K. S. Miller and B. Ross, *An Introduction to the Fractional Calculus and Fractional Differential Equations,* Wiley & Sons, New York, 1993.

[15] R. Hilfer, *Applications of Fractional Calculus in Physics,* World Scientific, Singapore, 2000.

[16] A. Oustaloup, *La Commande CRONE: Commande Robuste d'Ordre Non Entier,* Editions Hermès, Paris, 1991.

[17] Machado, J. A. T., *Discrete-Time Fractional-Order Controllers,* FCAA J. of Fractional Calculus & Applied Analysis Vol. 4; pp. 47–66, 2001.